Typeset using LaTeX default style in AASTeX631

A Test of the Gaussian Plasma Lens Model on an Extreme Scattering Event Toward PSR J2313+4253

Zachary C. Zelensky [1]

[1] Department of Physics and Astronomy, Texas Tech University, Lubbock, TX, 79409 USA

ABSTRACT

We present a test of the Gaussian plasma lens model for an extreme scattering event (ESE) toward PSR J2313+4253. This event was observed using high-cadence observations taken with the Green Bank Observatory 20m telescope. The high density of observations in time allow the event to be tracked in unprecedented detail. We observe a pair of caustic spikes along with the characteristic drop in scintillation bandwidth that is expected during an ESE. This pattern coincides with a sudden change in the estimated scattering screen distance. This project consists of an MCMC analysis to identify the lens parameters that best fit the trend seen in the scintillation bandwidth measurements. This analysis is compared with the results from SciPy's optimize function. Through these analyses, we can determine the significance of the event compared to the nominal distribution expected along the line of sight. This project was selected because it provides an opportunity to work on an interesting application of class material for my own data set. The results may be implemented into a paper on the event, that is in preparation.

Keywords: Stars: pulsars – ISM: general — ISM: structure

1. INTRODUCTION

Pulsar Scintillation provides a useful method to probe AU-parsec scale structures in the ionized interstellar medium (ISM). Scintillation arises as the multipath radio emission from a pulsar interacts with free electrons at a scattering screen along the line of sight. When this occurs, there is a phase shift in the photons from with differing path lengths. Photons redirected toward Earth recombine at a telescope, creating an interference pattern that evolves in frequency and time. This interference pattern is seen in the pulsar's dynamic spectrum, which shows flux density as a function of frequency and time, and manifests as regions of constructive inference, known as scintles. (Stinebring et al. 2001).

Extreme scattering events (ESEs), were first observed as flux density variations of quasars, likely originating from small-scale variations in the (ISM) (Fiedler et al. 1987). When an ESE is observed, there is a sudden frequency-dependent change in the observed flux, creating caustic spikes, as rays pile up at the edges of the lens, and a dip in the center, as the rays are defocused. The magnitude of the flux decrease, as well as the distance between these spikes, can be useful in determining properties of the ESE source.

ESEs are also present in observations of pulsars, with the first such event observed toward the millisecond pulsar B1937+21 (Cognard et al. 1993). ESEs can be tracked in pulsar observations through several quantities, including flux variations, changes in dispersion measure (DM), which is the integrated column density of free electrons along the line of sight, scintillation bandwidth and timescale, which are the width of the observed scintles in frequency and time, respectively, inferred scattering screen distance, or angular broadening measurements. Many times there is a simultaneous trend in two or more of these parameters. For example, several ESEs have been detected with scintillation bandwidth and DM variations (Coles et al. 2015). Additionally, two ESEs have been detected with flux density and scintillation bandwidth variations (Kerr et al. 2017). These events can range in duration from several weeks to a few years, with the longest recorded lasting 3 years (Maitia et al. 2003).

Several models have been proposed to explain the structural origins of ESEs. One such explanation models the ESE's source as a Gaussian plasma lens (Clegg et al. 1998). Plasma lenses are diverging lenses; this creates a drop in intensity near the center of the lens and causes light rays to pile up at the edges, forming caustics.

In this paper, we test the Gaussian plasma lens model on an ESE detected toward PSR J2313+4253. In Section 2, we discuss the dataset used. In Section 3, we fit the model to the data and provide analyses. In Section 4, we discuss the conclusions of this project.

2. DATA

The data for this project was sourced from my own observations taken with the Green Bank Observatory 20m telescope as part of the PSC Scintillation Survey (Turner et al. 2024). The observations are 2 hours in length with the "all" filter enabled, giving a frequency range of 1350-1750 MHz. This filter allows for the widest possible observing bandwidth, which provides tighter constraints on scintillation parameter estimates. We have a near-biweekly observing cadence during our observing campaign. This was increased to a near-weakly cadence when it became apparent that a potential ESE was occurring. The sampling time was 4.18 ms and ephemerides were taken from the Australia National Telescope Facility (ATNF) pulsar catalog (Manchester et al. 2005).

In order to remove radio frequency interference (RFI), excision was performed using a custom median-smoothed zapping script, as well as manual removal of individual pixels. Once RFI was removed the data spanned around 170 MHz centered near 1435 MHz. After folding and summing the data over polarizations, depending on the signal-to-noise ratio (S/N) of each observation, our data was averaged in frequency to yield channels of either 1 or 0.5 MHz (512 and 1024 frequency channels, respectively) across the observing band. The data was averaged in time with subintegrations ranging from 10-30 seconds, with the lower resolution being used to for particularly low S/N observations, in order to complete scintillation analyses.

The scintillation parameters were calculated for each of the observations following the procedure in Turner et al. (2024). In Figure 1, we present a time series of the scintillation bandwidth for each epoch. Before the event, the value of $\Delta\nu_{\rm d}$ fluctuates randomly around a mean value. The ESE is first seen around MJD 60306, where there is a sharp drop in $\Delta\nu_{\rm d}$. The scintillation bandwidth then rises to a caustic spike, followed by another drop. The event then produces another spike and continues to fall until MJD 60528. Using an unpaired t-test, a statistical test which can be used to determine if the mean of two groups is significantly different, for the values in the boxed region vs unboxed region yields a p-value of 0.043 for bandwidth. This is statistically significant, which means that the values are drawn from different distributions.

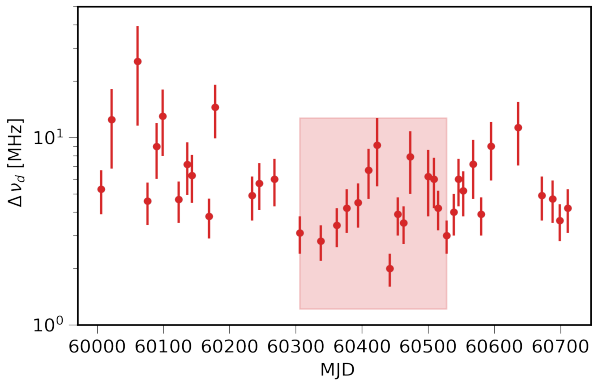

Figure 1. A time-series of the measured scintillation bandwidths $\Delta\nu_{\rm d}$ The shaded region indicates the duration over which the ESE takes place.

3. ESE MODEL

An expression for the gain of light rays passing through a Gaussian plasma lens (Gpl) is given by

$$G = [1 + (1 - 2bu^2)\alpha exp(-bu^2)]^{-1} + C, \tag{1}$$

where α is a lens parameter and u represents the ray path (Clegg et al. 1998). We have introduced the additional parameters b, to scale the distance between caustic spikes, and C to account for uncertainty. For simplicity we are

only considering a single ray path. Since we are fitting over scintillation bandwidth instead of magnification, any fitted parameters don't necessarily have a physical meaning; however, we expect any trends seen in scintillation bandwidth to closely follow the behavior in flux density.

3.1. *SciPy Optimize*

Using the Gpl model, we can fit Equation 2 to our scintillation bandwidth measurements taken during the event (boxed region in Figure 1) using SciPy's optimize function (Virtanen et al. 2020). Before fitting, the data was first centered, so that modified MJD 0 was in the middle of the two caustic spikes, and then scaled by dividing each value by the first event bandwidth measurement at MJD 60306. The result of the fit is shown in Figure 2. The optimal parameters are $\alpha = 1.47$, $b = 0.04$, and $C = 0.34$, resulting in $\chi^2_{dof} = 1.44$. This means that the model with the optimal parameters slightly under-fits the data, however; the model is still successful at capturing the overall trend.

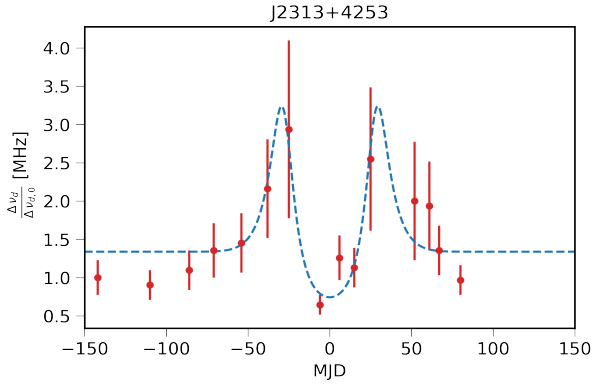

Figure 2. A fit of the Gaussian plasma lens model using SciPy's optimize function (dashed blue line) for the scintillation bandwidth values during the event.

3.2. *MCMC*

The same analysis can be completed using an MCMC to sample the parameter space. This was achieved using Ultranest's reactive nested sampler (Buchner 2021). To set up the analysis, a uniform prior was used for each of the parameters, with a Gaussian likelihood function and 400 live sampling points. The posterior distribution for each parameter is shown in Figure 3. The optimal parameters are $\alpha = 1.12 \pm 0.37$, $b = 0.04 \pm 0.0088$, and $C = 0.34 \pm 0.074$. This method agrees within 1 sigma with the results of the frequentist approach we used in Section 3.1. The fit of these parameters, in the Gpl model, is shown in Figure 4. The optimal parameters are plotted with the solid black line, with the 1 sigma quantile shaded in dark grey.

This fit can be compared to the pure noise model that simulates random variation about a constant value. This model is given by

$$y = D, \tag{2}$$

where D is a constant parameter. Using the same MCMC analysis for this model yields the optimal value $D = 1.005 \pm 0.073$. A comparison of the optimal parameter fits for each of these models is shown in Figure 5. Computing the Bayes factor for the Gpl model vs the pure noise model finds that the Gpl model is 323.22 times more probable. This is very strong evidence to prefer the Gpl model over pure noise. For both techniques, our data is well modeled by the Gaussian plasma lens. This adds validity to the event and provides a successful test of the model.

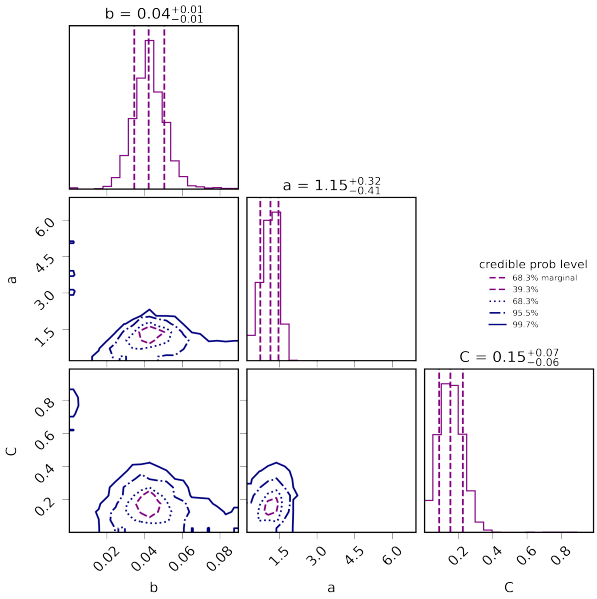

Figure 3. A corner plot showing the MCMC results for the posterior distribution for the parameters and their corresponding credible regions.

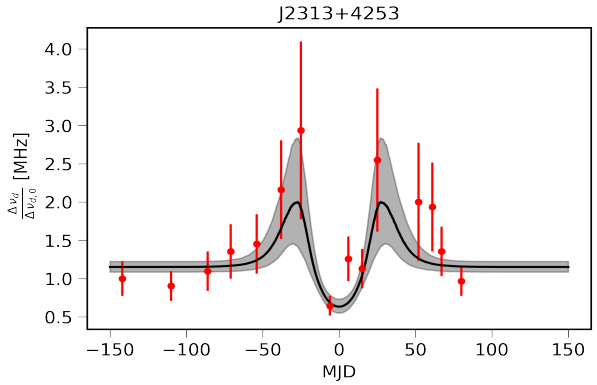

Figure 4. A fit of the Gaussian plasma lens model (black line) for the scintillation bandwidth values during the event found using the MCMC. The shaded region corresponds to values within the 1 sigma credible regions.

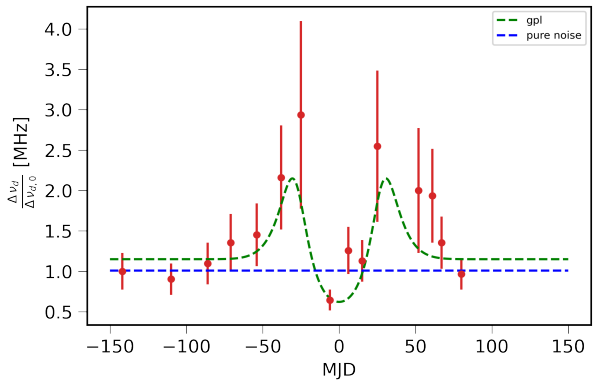

Figure 5. A comparison of the fit from the Gaussian plasma lens (dashed green line) and the pure noise model (dashed blue line).

4. CONCLUSIONS & FUTURE WORK

We have provided a test of the Gaussian plasma lens model with both Frequentist and Bayesian approaches. In both cases the data is well modeled and both approaches agree on the optimal parameters. The Gpl model is strongly preferred over pure noise, this provides credibility to the event and sheds light on the structural origins of ESEs.

Future tests of additional models could future constrain the structural origins of ESEs. With future monitoring of scintillation parameters for more pulsars, additional ESEs may be identified. Telescopes that continuously monitor pulsars could be used as an ESE detection system. This would allow for a higher detection rate. Once an ESE is identified, triggered proposals could be used to gather high-resolution data. Tracking these events with high cadence allows for a detailed analysis of these events. This will help to further constrain and test theories for the origins of these events.

Software: psrchive (Hotan et al. 2004), pypulse (Lam 2017), scipy (Virtanen et al. 2020), numpy (van der Walt et al. 2011), matplotlib (Hunter 2007) , ultranest (Buchner 2021)

REFERENCES

Buchner, J. 2021, UltraNest – a robust, general purpose Bayesian inference engine. https://arxiv.org/abs/2101.09604

Clegg, A. W., Fey, A. L., & Lazio, T. J. W. 1998, ApJ, 496, 253, doi: 10.1086/305344

Cognard, I., Bourgois, G., Lestrade, J., et al. 1993, Nature, 366, doi: 10.1038/366320a0

Coles, W. A., Kerr, M., Shannon, R. M., et al. 2015, ApJ, 808, 113, doi: 10.1088/0004-637X/808/2/113

Fiedler, R. L., Dennison, B., Johnston, K. J., & Hewish, A. 1987, Nature, 326, 675, doi: 10.1038/326675a0

Hotan, A. W., van Straten, W., & Manchester, R. N. 2004, PASA, 21, 302, doi: 10.1071/AS04022

Hunter, J. D. 2007, Computing in Science and Engineering, 9, 90, doi: 10.1109/MCSE.2007.55

Kerr, M., Coles, W. A., Ward, C. A., et al. 2017, Monthly Notices of the Royal Astronomical Society, 474, 4637, doi: 10.1093/mnras/stx3101

Lam, M. T. 2017, PyPulse: PSRFITS handler, Astrophysics Source Code Library, record ascl:1706.011

Maitia, V., Lestrade, J. F., & Cognard, I. 2003, ApJ, 582, 972, doi: 10.1086/344816

Manchester, R. N., Hobbs, G. B., Teoh, A., & Hobbs, M. 2005, AJ, 129, 1993, doi: 10.1086/428488

Stinebring, D. R., McLaughlin, M. A., Cordes, J. M., et al. 2001, The Astrophysical Journal, 549, L97, doi: 10.1086/319133

Turner, J. E., Medina, J. G. L., Zelensky, Z., et al. 2024, The Astrophysical Journal, 977, 205, doi: 10.3847/1538-4357/ad9008

van der Walt, S., Colbert, S. C., & Varoquaux, G. 2011, Computing in Science and Engineering, 13, 22, doi: 10.1109/MCSE.2011.37

Virtanen, P., Gommers, R., Oliphant, T. E., et al. 2020, Nature Methods, 17, 261, doi: 10.1038/s41592-019-0686-2